IEEE Access
Multidisciplinary | Rapid Review | Open Access Journal

Received June 10, 2019, accepted July 8, 2019, date of publication July 15, 2019, date of current version July 31, 2019.

Digital Object Identifier 10.1109/ACCESS.2019.2928851

A DOA-Based Factor Graph Technique for 3D Multi-Target Geolocation

MENG CHENG[1], (Member, IEEE), MUHAMMAD REZA KAHAR AZIZ[2], (Member, IEEE), AND TAD MATSUMOTO[1,3], (Fellow, IEEE)

[1]School of Information Science, Japan Advanced Institute of Science and Technology, Ishikawa 923-1211, Japan
[2]School of Electrical Engineering, Institut Teknologi Sumatera, Lampung Selatan 35365, Indonesia
[3]Center for Wireless Communications, University of Oulu, 90014 Oulu, Finland

Corresponding author: Meng Cheng (m-cheng@jaist.ac.jp)

This work was supported in part by the Hitachi, Ltd., and in part by the Hitachi Kokusai Electric Inc.

ABSTRACT The primary goal of this paper is to propose a new factor graph (FG) technique for the direction-of-arrival (DOA)-based three-dimensional (3D) multi-target geolocation. The proposed FG detector uses only the mean and the variance of the DOA measurement including both the azimuth and the elevation, assuming that they are suffering from errors following a Gaussian probability density function (PDF). Therefore, both the up-link (UL) transmission load and the detection complexity can be significantly reduced. The Cramer–Rao lower bound (CRLB) of the proposed DOA-based 3D geolocation system is mathematically derived. According to the root mean square error (RMSE) results obtained by simulations, the proposed FG algorithm is found to outperform the conventional linear least square (LS) approach, which achieves a very close performance to the derived CRLB. Moreover, we propose a sensor separation algorithm to solve the target-DOAs matching problem such that the DOAs, measured by each sensor, can be matched to their corresponding targets. With this technique, additional target identification is not needed, and the multi-target geolocation can be decomposed into multiple independent single-target detections.

INDEX TERMS 3D geolocation, direction of arrival (DOA), factor graph (FG), CRLB, anonymous multi-target geolocation, sensor separation algorithm, target-DOAs matching.

I. INTRODUCTION

As one of the enabling technologies of building a smart city, wireless geolocation with densely distributed sensors is expected to play an important role in the future network functionalities [1]. The applications may include low-power wide-area networks (LPWAN), unmanned factories, vehicle-to-everything (V2X) communication systems [2] and etc. However, due to the explosive growth of service demands, the wireless up-link (UL) communication in a fully centralized network will very likely cause a transmission flooding problem. Therefore, pre-processing having relatively light computations at the distributed sensors is believed to alleviate the UL traffic load and reduce the computational burden at the fusion center [3], [4]. As one of the solutions, factor graph (FG) algorithm was first proposed to solve the wireless geolocation problem in [5], where sensors are capable of extracting only key parameters of the probability density function (PDF) of the measured time-of-arrival (TOA). With the Gaussian assumption of the measurement errors, only the mean and variance of the TOAs are transmitted from sensors to the fusion center, which significantly saves the UL transmission load. Moreover, the massages passed in the FG detector are also Gaussian-approximated, and therefore the required computational complexity at the fusion center is very low [6]. The performance gain of the FG detector over conventional techniques has been found in many literatures, e.g., [5], [7].

Due to the advantages of FG, many extensions of [5] have been proposed for the range-based geolocation [8], such as the modified algorithm with TOA [9], the received signal strength (RSS) [10], [11], the time difference of arrival (TDOA) [12] and the direction of arrival (DOA) [13]. Since the objective of this paper is to detect anonymous targets, such as the illegal radio emitter, keeping time synchronization between sensors and targets is generally impossible, which is needed in the TOA-based technique. For the RSS-based technique, it is impossible to make correspondence between the anonymous target RSS and the reference RSS obtained through the off-line training [7]. Even though TDOA can

The associate editor coordinating the review of this manuscript and approving it for publication was Shihao Yan.

avoid the necessity of synchronization, it is very sensitive to the measurement error because the radio signal propagates at the light speed. Moreover, TDOA can not be measured if the target has a silent period of time, i.e., no signal is emitted. To avoid such technical limitations, this paper focuses on the DOA-based geolocation. The primary reason is that no time synchronization is required for DOA measurement at the sensors. Furthermore, if a mapping rule between the image coordinate points and the DOAs is established, digital cameras can be used to measure the DOA of silent targets [14], where the multi-path impact can be completely eliminated. Considering the 5G development, the future device deployment will become denser, and the line-of-sight (LOS) links between targets and the surrounding sensors are supposed to increase. Moreover, due to the characteristic of millimeter-wave (mmWave) propagation, the signal attenuation is very serious, and the multi-path effect will be significantly reduced [15]. Therefore, we believe that the DOA-based techniques are more suitable for positioning services in the future 5G network.

Many techniques have been proposed for measuring DOAs, such as MUSIC, ESPRIT and SAGE [16], [17]. For example, a linear array is utilized in [18] with the alternate elements orthogonally polarized, such that the estimation of azimuth/elevation angles can be conducted by only one-dimensional search in the MUSIC algorithm. In [19], a separable sparse representation (SSR-DOA) algorithm is proposed, which splits the joint azimuth/elevation observation matrix into two individual sub-matrices, in order to reduce the estimation complexity. Current DOA measuring techniques solve not only the single target, but also the multiple targets, such as in [20]. In the multi-target case, a pair-matching approach [21] is applied at each sensor, to associate the azimuth and the elevation corresponding to the same target. The techniques described above make the assumptions of this paper more realistic, where each of the distributed sensors is capable of measuring the azimuth/elevation in the multi-target case, with perfect pair-matching. Note that the objective of this paper is to use DOAs for geolocation, and therefore discussing specific DOA measuring technique is beyond the scope of this paper.

Reference [7] provides a solid work of DOA-based geolocation with FG for single-target in a 2-dimensional (2D) plane. However, it may not be usable in many practical applications, e.g., drone detection, automation factory and self-driving automobile, where 3D positioning, tracking and multi-target detection are needed. To satisfy such requirements in future networks, this paper proposes a new DOA-based FG technique for 3D anonymous multi-target geolocation. Specifically, both the azimuth and the elevation measured at each sensor are taken into account in the proposed FG detector, where new factor nodes are introduced to connect the both angles to the position parameters in the standard 3D coordinate. To guarantee the distribution Gaussianity of the messages passed in FG, the first-order Taylor series (TS) expansion of trigonometric functions is used. It should be noted that the convergence proof of the FG-based geolocation techniques is expected to be very difficult, as pointed out by the pioneer work in [22]. Therefore, the convergence property in terms of root mean squared error (RMSE) is only evaluated by the simulations. The robustness of the proposed technique is also evaluated in terms of iteration time, snapshot number and standard deviation of the measurement errors.

Besides the range-based single-target detection, many geolocation techniques have been proposed for the multi-target case. For example, [23] combines the orthogonal frequency division multiplexing (OFDM) technique with radar to separate DOAs coming from different targets at the sensor. In [24], a non-orthogonal transmission of DOA is applied for a MIMO radar system, where the maximum detectable target number is also investigated. Multiple sensers are used in [25] for the TOA-based multi-target detection, and the transmission schemes between sensors and targets are assumed to be known, resulting in the fact that the target identification is equivalent to a wireless multiple access problem. However, the techniques described above may not be applicable for the next generation geolocation system due to three reasons: (1) massively deployed sensors in the future network are expected to be cheap, where complicated hardwares may not be equiped; (2) targets may be anonymous, and conventioanl identification techniques used in wireless communications, e.g., the target-specific reference signal, may not be available; (3) although multi-target DOA estimation can be conducted at every individual sensor, techniques for matching between the DOAs, measured by each sensor, and their corresponding targets are not yet known. This problem is referred to as a target-DOAs matching problem in this paper. Note that [26] and [27] propose techniques to solve the matching problem in a dynamic model, where the time-domain correlation is utilized. Instead, our goal is the stationary target detection, without requiring any time-domain a priori information.

Motivated by the problems described above, this paper provides a simple but yet useful solution for anonymous multi-target detection with distributed sensors. The key idea is to solve the target-DOAs matching problem beforehand, such that the multi-target geolocation can be decomposed into multiple independent single-target detections, each conducting the proposed FG algorithm. This idea is realized by the proposed sensor separation algorithm, without relying on conventional identification techniques, such as the target-specific reference signal. To the best of our knowledge, no previous work is found related to our proposed technique. The main contributions of this paper are summarized as follows.

1) A new DOA-based FG algorithm is proposed for 3D geolocation, which exhibits clear robusteness and performance gain over the conventional linear least square (LS) approach [28].
2) The Cramer-Rao lower bound (CRLB) is mathematically derived as the performance reference of the proposed DOA-based 3D geolocation system.

3) A sensor separation algorithm is proposed for the multi-target case, which provides matching information between the originating target and measured DOAs at different sensors. Therefore, the multi-target geolocation can be decomposed into multiple independent single-target detections, such that the computational complexity is almost linear to the target number. The conventional identification techniques, such as target-specific reference signal, are also avoided.

The organization of this paper is as follows. In Section II, the assumptions used in the geolocation system model is introduced. The proposed FG algorithm for DOA-based 3D geolocation is then described in Section III. In Section IV, the CRLB of the proposed system is mathematically derived. The accuracy of single-target detection using the proposed technique is verified in Section V through simulations. Moreover, the sensor separation algorithm is introduced in Section VI for target-DOAs matching in the multi-target case. The simulation results evaluating the performance of the proposed technique is also included. Finally, this work is concluded in Section VII with some concluding remarks.

II. SYSTEM MODEL

In the proposed geolocation system, a global 3D sphere coordinate is used to describe the locations of sensors and targets. First of all, N anonymous targets are assumed within the sensing area, locating at $g_n = [x_n, y_n, z_n]^T$, where $n = \{1, \ldots, N\}$, and $[\cdot]^T$ denotes the transposed matrix or vector of its argument. Meanwhile, the locations of M distributed sensors $G_m = [X_m, Y_m, Z_m]$ are known by the fusion center, where $m = \{1, \ldots, M\}$. Therefore, the relative distance $\Delta d_{m,n}$ between the m-th sensor and the n-th target can be calculated by

$$d_{m,n} = \begin{bmatrix} \Delta x_{m,n} \\ \Delta y_{m,n} \\ \Delta z_{m,n} \end{bmatrix} = \begin{bmatrix} X_m \\ Y_m \\ Z_m \end{bmatrix} - \begin{bmatrix} x_n \\ y_n \\ z_n \end{bmatrix}. \tag{1}$$

For each sensor, the received DOA can be decomposed into two domains, i.e., the azimuth φ and the elevation θ, both following the standard definition of the spherical coordinate shown in Fig. 1. By ignoring the subscripts of variables for the seek of simplicity, the connections of such relative distances can be expressed by

$$\begin{aligned} \Delta x &= \Delta y \cdot \tan(\varphi) && (2)\\ &= \Delta z \cdot \sin(\varphi) \cdot \tan(\theta), && (3)\\ \Delta y &= \Delta x \cdot \cot(\varphi) && (4)\\ &= \Delta z \cdot \cos(\varphi) \cdot \tan(\theta), && (5)\\ \Delta z &= \Delta x \cdot \sec(\varphi) \cdot \cot(\theta) && (6)\\ &= \Delta y \cdot \csc(\varphi) \cdot \cot(\theta). && (7) \end{aligned}$$

It is found that the relative distance variables in the equations (2)-(7) are self-contained, and therefore the iterative message passing algorithm using FG can be applied to detect them. Moreover, every relative distance variable can be calculated by two different functions, which indicates their connections to two factor nodes in the proposed FG structure, as detailed in the next section. In addition, sensors are assumed to capture the DOA measurements with L snapshots, influenced by the errors following Gaussian distribution, as

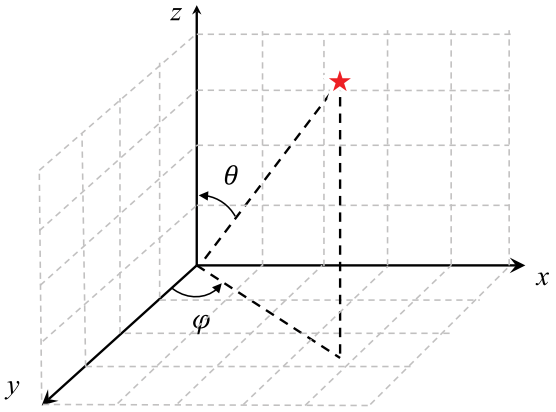

FIGURE 1. Definition of the azimuth φ and the elevation θ in the 3D sphere coordinate.

$$\varphi_l = \varphi + n_{\varphi,l}, \quad l = \{1, 2, \ldots, L\}, \tag{8}$$

$$\theta_l = \theta + n_{\theta,l}, \quad l = \{1, 2, \ldots, L\}, \tag{9}$$

where the noise components $n_\varphi \sim \mathcal{N}(0, \sigma_\varphi^2)$ and $n_\theta \sim \mathcal{N}(0, \sigma_\theta^2)$, respectively. It should be noted that the transmission channels between sensors and the fusion center are assumed to be error-free, and hence no specific transmission scheme is considered for the UL. Moreover, the quantization errors, which may appear when applying digital camera sensors, are included in the noise terms of (8)-(9), because they are assumed to be sufficiently small in this paper.

III. PROPOSED FG ALGORITHM

In this section, detailed discussions of the DOA-based 3D geolocation is provided, with the proposed FG detector shown in Fig. 2. For the sake of simplicity, the subscripts of variables indicating the sensor index are omitted in the following contents. First of all, the means and variances of the measured azimuth/elevation are calculated by the measurement factor nodes (D_φ, D_θ) at each sensor, i.e., $(m_\varphi, \sigma_\varphi^2)$ and $(m_\theta, \sigma_\theta^2)$. They are then sent from the angle variable nodes (N_φ, N_θ) to the trigonometric factor node (F_A, F_B, F_C) at the fusion center, which initiates the iterative detection.

It should be noted that F_A takes only the azimuth angle φ, and connects the variable nodes Δx and Δy according to (2) and (4). The utilization of F_A is sufficient for detecting the target's position in X-Y plane, as shown in the 2D geolocation in [7]. However, in the 3D geolocation, the elevation angle is also included to further connect Δx and Δy to Δz. In this paper, two new factor nodes are introduced, where F_B connects Δx and Δz according to (3) and (6), and F_C connects Δy and Δz according to (5) and (7), respectively. Therefore, every variable node of the relative distance is connected to two different trigonometric factor nodes, as mentioned in the previous section.

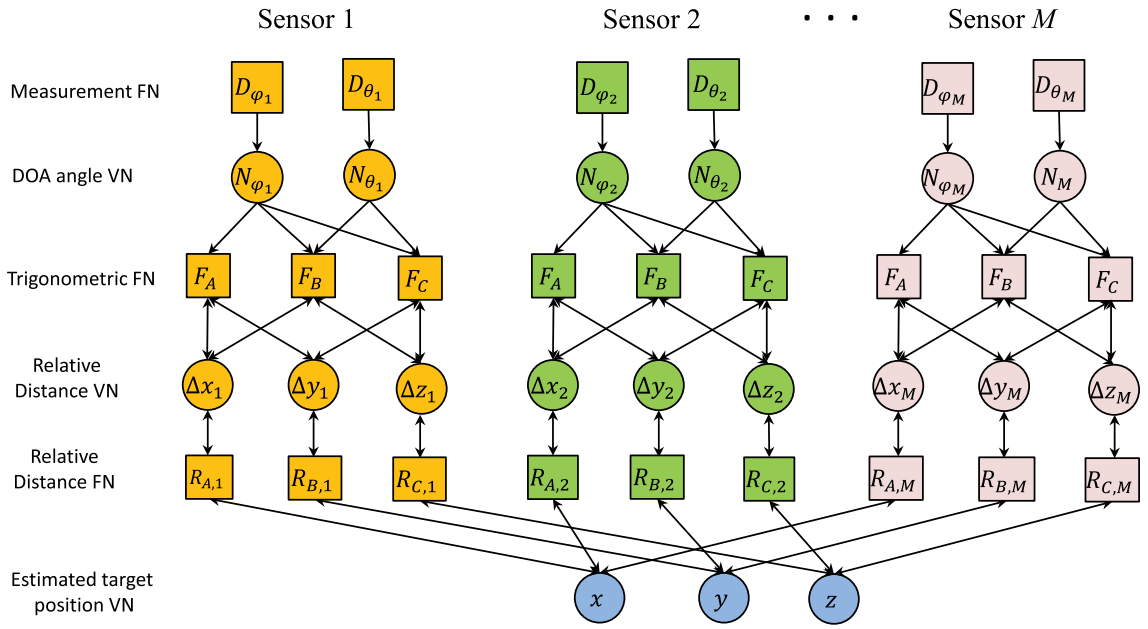

FIGURE 2. Proposed FG detector for the DOA-based 3D geolocation.

According to (2)-(7), multiplications of two independent variables are involved in F_A, and multiplications of three independent variables are involved in F_B and F_C. Due to the Gaussian assumption of the messages, only the mean and the variance need to be updated in the factor nodes. For example, for two independent variables $a \sim \mathcal{N}(m_a, \sigma_a^2)$ and $b \sim \mathcal{N}(m_b, \sigma_b^2)$, the mean and the variance of their product $a \cdot b$ can be calculated by

$$m_{a\cdot b} = m_a \cdot m_b, \tag{10}$$
$$\sigma_{a\cdot b}^2 = m_a^2 \cdot \sigma_b^2 + m_b^2 \cdot \sigma_a^2 + \sigma_a^2 \cdot \sigma_b^2. \tag{11}$$

Similarly, by introducing a third variable $c \sim \mathcal{N}(m_c, \sigma_c^2)$, the product of three independent variables $a \cdot b \cdot c$ will have

$$m_{a\cdot b\cdot c} = m_a \cdot m_b \cdot m_c, \tag{12}$$
$$\begin{aligned}\sigma_{a\cdot b\cdot c}^2 = {} & m_a^2 \cdot m_c^2 \cdot \sigma_b^2 + m_b^2 \cdot m_c^2 \cdot \sigma_a^2 + m_a^2 \cdot m_b^2 \cdot \sigma_c^2 \\ & + m_a^2 \cdot \sigma_b^2 \cdot \sigma_c^2 + m_b^2 \cdot \sigma_a^2 \cdot \sigma_c^2 + m_c^2 \cdot \sigma_a^2 \cdot \sigma_b^2 \\ & + \sigma_a^2 \cdot \sigma_b^2 \cdot \sigma_c^2.\end{aligned} \tag{13}$$

However, it has to be noted that since the trigonometric functions in (2)-(7) are not linear, the Gaussian assumption does not hold for their calculations. To deal with this problem, the first-order TS expansion is used as a linear approximation of the trigonometric functions given by

$$f(\alpha) \approx f(m_\alpha) + f'(m_\alpha)(\alpha - m_\alpha). \tag{14}$$

In (14), $f(\alpha)$ denotes the original function of the variable α, which is linearly approximated at $\alpha = m_\alpha$, where $f(m_\alpha)$, $f'(m_\alpha)$ and m_α are all constants. Therefore, the mean and the variance of the approximated function can be given by

$$m_{f(\alpha)} \approx f(m_\alpha), \tag{15}$$
$$\sigma_{f(\alpha)}^2 \approx \left[f'(m_\alpha)\right]^2 \cdot \sigma_\alpha^2. \tag{16}$$

By following (15) and (16), the means and the variances of the trigonometric functions in (2)-(7) can be approximated as shown in Table 1.

TABLE 1. Approximated means and variances of related trigonometric functions.

	Approximated mean	Approximated variance
$\tan(\alpha)$	$\tan(m_\alpha)$	$\sec^4(m_\alpha) \cdot \sigma_\alpha^2$
$\cot(\alpha)$	$\cot(m_\alpha)$	$\csc^4(m_\alpha) \cdot \sigma_\alpha^2$
$\sin(\alpha)$	$\sin(m_\alpha)$	$\cos^2(m_\alpha) \cdot \sigma_\alpha^2$
$\cos(\alpha)$	$\cos(m_\alpha)$	$\sin^2(m_\alpha) \cdot \sigma_\alpha^2$
$\sec(\alpha)$	$\sec(m_\alpha)$	$\sec^2(m_\alpha) \cdot \tan^2(m_\alpha) \cdot \sigma_\alpha^2$
$\csc(\alpha)$	$\csc(m_\alpha)$	$\csc^2(m_\alpha) \cdot \cot^2(m_\alpha) \cdot \sigma_\alpha^2$

With the mathematical preparations described above, the proposed iterative FG algorithm is detailed as follows. First of all, the message flow will start from the trigonometric factor nodes to the relative distance variable nodes. According to the proposed FG structure shown in Fig. 2, there are two trigonometric factor nodes having independent message flows to the same relative distance variable node, and each coming message is assumed to be independently Gaussian distributed. With such assumption, the PDF of the resulted message is a product of two independent Gaussian PDFs, which is also Gaussian, i.e.,

$$\mathcal{N}\left(m_a, \sigma_a^2\right) \times \mathcal{N}\left(m_b, \sigma_b^2\right) = \mathcal{N}\left(\frac{m_a\sigma_b^2 + m_b\sigma_a^2}{\sigma_a^2 + \sigma_b^2}, \frac{1}{\frac{1}{\sigma_a^2} + \frac{1}{\sigma_b^2}}\right). \tag{17}$$

Therefore, the means and variances of the messages passing from the relative distance variable nodes to the relative

distance factor nodes can be calculated according to (17), which are given by,

$$m_{\Delta x\to R_A} = \frac{m_{F_A\to\Delta x}\cdot\sigma^2_{F_B\to\Delta x}+m_{F_B\to\Delta x}\cdot\sigma^2_{F_A\to\Delta x}}{\sigma^2_{F_A\to\Delta x}+\sigma^2_{F_B\to\Delta x}}, \quad (18)$$

$$m_{\Delta y\to R_B} = \frac{m_{F_A\to\Delta y}\cdot\sigma^2_{F_C\to\Delta y}+m_{F_C\to\Delta y}\cdot\sigma^2_{F_A\to\Delta y}}{\sigma^2_{F_A\to\Delta y}+\sigma^2_{F_C\to\Delta y}}, \quad (19)$$

$$m_{\Delta z\to R_C} = \frac{m_{F_B\to\Delta z}\cdot\sigma^2_{F_C\to\Delta z}+m_{F_C\to\Delta z}\cdot\sigma^2_{F_B\to\Delta z}}{\sigma^2_{F_B\to\Delta z}+\sigma^2_{F_C\to\Delta z}}, \quad (20)$$

and

$$\sigma^2_{\Delta x\to R_A} = \frac{1}{\frac{1}{\sigma^2_{F_A\to\Delta x}}+\frac{1}{\sigma^2_{F_B\to\Delta x}}}, \quad (21)$$

$$\sigma^2_{\Delta y\to R_B} = \frac{1}{\frac{1}{\sigma^2_{F_A\to\Delta y}}+\frac{1}{\sigma^2_{F_C\to\Delta y}}}, \quad (22)$$

$$\sigma^2_{\Delta z\to R_C} = \frac{1}{\frac{1}{\sigma^2_{F_B\to\Delta z}}+\frac{1}{\sigma^2_{F_C\to\Delta z}}}. \quad (23)$$

The means of the separated message passing from the trigonometric factor node to the relative distance variable node can be easily derived by

$$m_{F_A\to\Delta x} = m_{\Delta y\to F_A}\cdot\tan\left(m_\varphi\right), \quad (24)$$

$$m_{F_B\to\Delta x} = m_{\Delta z\to F_B}\cdot\sin\left(m_\varphi\right)\cdot\tan\left(m_\theta\right), \quad (25)$$

$$m_{F_A\to\Delta y} = m_{\Delta x\to F_A}\cdot\cot\left(m_\varphi\right), \quad (26)$$

$$m_{F_C\to\Delta y} = m_{\Delta z\to F_C}\cdot\cos\left(m_\varphi\right)\cdot\tan\left(m_\theta\right), \quad (27)$$

$$m_{F_B\to\Delta z} = m_{\Delta x\to F_B}\cdot\sec\left(m_\varphi\right)\cdot\cot\left(m_\theta\right), \quad (28)$$

$$m_{F_C\to\Delta z} = m_{\Delta y\to F_C}\cdot\csc\left(m_\varphi\right)\cdot\cot\left(m_\theta\right). \quad (29)$$

Moreover, the variance to be forwarded from the F_A node to the Δx node can be given by

$$\begin{aligned}\sigma^2_{F_A\to\Delta x} = {} & m^2_{\Delta y\to F_A}\cdot\sec^4\left(m_\varphi\right)\cdot\sigma^2_\varphi \\ & +\tan^2\left(m_\varphi\right)\cdot\sigma^2_{\Delta y\to F_A} \\ & +\sigma^2_{\Delta y\to F_A}\cdot\sec^4\left(m_\varphi\right)\cdot\sigma^2_\varphi,\end{aligned} \quad (30)$$

and the variance to be forwarded from the F_B node to the Δx node is

$$\begin{aligned}\sigma^2_{F_B\to\Delta x} = {} & m^2_{\Delta z\to F_B}\cdot\tan^2\left(m_\theta\right)\cdot\cos^2\left(m_\varphi\right)\cdot\sigma^2_\varphi \\ & +\sin^2\left(m_\varphi\right)\cdot\tan^2\left(m_\theta\right)\cdot\sigma^2_{\Delta_z\to F_B} \\ & +m^2_{\Delta z\to F_B}\cdot\sin^2\left(m_\varphi\right)\cdot\sec^4\left(m_\theta\right)\cdot\sigma^2_\theta \\ & +m^2_{\Delta z\to F_B}\cdot\cos^2\left(m_\varphi\right)\cdot\sigma^2_\varphi\cdot\sec^4\left(m_\theta\right)\cdot\sigma^2_\theta \\ & +\sin^2\left(m_\varphi\right)\cdot\sigma^2_{\Delta_z\to F_B}\cdot\sec^4\left(m_\theta\right)\cdot\sigma^2_\theta \\ & +\tan^2\left(m_\theta\right)\cdot\sigma^2_{\Delta_z\to F_B}\cdot\cos^2\left(m_\varphi\right)\cdot\sigma^2_\varphi \\ & +\sigma^2_{\Delta_z\to F_B}\cdot\cos^2\left(m_\varphi\right)\cdot\sigma^2_\varphi\cdot\sec^4\left(m_\theta\right)\cdot\sigma^2_\theta.\end{aligned} \quad (31)$$

Due to the space limitation, the rest of the variance calculations are omitted. However, they can be derived in similar ways to (30) and (31). Obviously, many terms included in the mean and the variance calculations above are re-usable for the complexity reducing, which is not detailed in this paper. At the relative distance factor node, the messages passing to different directions can be expressed according to (1), by

$$\left(m_{R_A\to x},\sigma^2_{R_A\to x}\right) = \left(X-m_{\Delta x\to R_A},\sigma^2_{\Delta x\to R_A}\right), \quad (32)$$

$$\left(m_{R_B\to y},\sigma^2_{R_B\to y}\right) = \left(Y-m_{\Delta y\to R_B},\sigma^2_{\Delta y\to R_B}\right), \quad (33)$$

$$\left(m_{R_C\to z},\sigma^2_{R_C\to z}\right) = \left(Z-m_{\Delta z\to R_C},\sigma^2_{\Delta z\to R_C}\right), \quad (34)$$

and

$$\left(m_{R_A\to\Delta x},\sigma^2_{R_A\to\Delta x}\right) = \left(X-m_{x\to R_A},\sigma^2_{x\to R_A}\right), \quad (35)$$

$$\left(m_{R_B\to\Delta y},\sigma^2_{R_B\to\Delta y}\right) = \left(Y-m_{y\to R_B},\sigma^2_{y\to R_B}\right), \quad (36)$$

$$\left(m_{R_C\to\Delta z},\sigma^2_{R_C\to\Delta z}\right) = \left(Z-m_{z\to R_C},\sigma^2_{z\to R_C}\right). \quad (37)$$

Note that the calculations shown above are performed in parallel for different sensors, and therefore the subscripts of the sensor index are omitted for the sake of simplicity. However, at the estimated target position variable node, the updated message has to be fed back to each parallel process as mentioned above to enable the FG iterations. Hence, the subscripts of sensor index are needed in the mean and the variance calculations, which are given by [29]

$$\frac{1}{\sigma^2_{x\to R_{A,m}}} = \sum_{i=1,i\neq m}^{M}\frac{1}{\sigma^2_{R_{A,i}\to x}}, \quad (38)$$

$$m_{x\to R_{A,m}} = \sigma^2_{x\to R_{A,m}}\cdot\sum_{i=1,i\neq m}^{M}\frac{m_{R_{A,i}\to x}}{\sigma^2_{R_{A,i}\to x}}. \quad (39)$$

The iterations are performed until certain conditions are met, e.g., the maximum iteration time is reached, or the gap between the estimated positions by two iterations is smaller than a pre-determined threshold. After that, the final estimations will be obtained by (43)-(45), where the variances σ^2_x, σ^2_y, and σ^2_z calculated from (40)-(42), respectively, are used.

$$\frac{1}{\sigma^2_x} = \sum_{i=1}^{M}\frac{1}{\sigma^2_{R_{A,i},\to x}}, \quad (40)$$

$$\frac{1}{\sigma^2_y} = \sum_{i=1}^{M}\frac{1}{\sigma^2_{R_{B,i},\to y}}, \quad (41)$$

$$\frac{1}{\sigma^2_z} = \sum_{i=1}^{M}\frac{1}{\sigma^2_{R_{C,i},\to z}}, \quad (42)$$

$$m_x = \sigma^2_x\cdot\sum_{i=1}^{M}\frac{m_{R_{A,i}\to x}}{\sigma^2_{R_{A,i},\to x}}, \quad (43)$$

$$m_y = \sigma^2_y\cdot\sum_{i=1}^{M}\frac{m_{R_{B,i}\to y}}{\sigma^2_{R_{B,i},\to y}}, \quad (44)$$

$$m_z = \sigma^2_z\cdot\sum_{i=1}^{M}\frac{m_{R_{C,i}\to z}}{\sigma^2_{R_{C,i},\to z}}. \quad (45)$$

IV. CRLB DERIVATION

In this section, the Cramer Rao lower bound (CRLB) for the DOA-based 3D geolocation is derived as the performance reference. According to [7], the CRLB is given by

$$\text{CRLB} = \sqrt{\text{trace}\left[F^{-1}(\mathbf{g})\right]}, \tag{46}$$

where F denotes the Fisher information matrix (FIM). Given the target position g and the PDF of the measured random variable $\hat{A}$, the FIM can be further rewritten by

$$F(g) = E\left[\left(\frac{\partial}{\partial g}\ln p\left(\hat{A}\right)\right)^2\right]. \tag{47}$$

where $\hat{A}$ denotes the DOA measurements for both the azimuth and the elevation with L samples, and $p(\cdot)$ is the PDF function. The final expression of the derived CRLB for the proposed DOA-based 3D geolocation system is then given by

$$\text{CRLB} = \sqrt{\text{trace}\left[\left(\mathbf{J}^T \Sigma_A^{-1} \mathbf{J}\right) L\right]^{-1}}, \tag{48}$$

where the Jacobian function $\mathbf{J}$ can be given by

$$\mathbf{J} = \begin{bmatrix} \frac{\Delta y_1}{\Delta xy_1{}^2} & -\frac{\Delta x_1}{\Delta xy_1{}^2} & 0 \\ \frac{\Delta y_2}{\Delta xy_2{}^2} & -\frac{\Delta x_2}{\Delta xy_2{}^2} & 0 \\ \vdots & \vdots & \vdots \\ \frac{\Delta x_1 \Delta z_1}{\Delta xyz_1{}^2 \Delta xy_1} & \frac{\Delta y_1 \Delta z_1}{\Delta xyz_1{}^2 \Delta xy_1} & -\frac{\Delta xy_1}{\Delta xyz_1{}^2} \\ \frac{\Delta x_2 \Delta z_2}{\Delta xyz_2{}^2 \Delta xy_2} & \frac{\Delta y_2 \Delta z_2}{\Delta xyz_2{}^2 \Delta xy_2} & -\frac{\Delta xy_2}{\Delta xyz_2{}^2} \\ \vdots & \vdots & \vdots \end{bmatrix}. \tag{49}$$

The detailed derivation of the CRLB can be seen in the appendix.

V. SINGLE-TARGET SIMULATIONS

A. COMPARATIVE LS APPROACH

In this section, the linear LS detection algorithm is presented for the DOA-based 3D geolocation for comparison. According to the equations in (2)-(7), the position estimate $[m_x, m_y, m_z]^T$ of the linear LS detector is given by

$$\begin{bmatrix} m_x \\ m_y \\ m_z \end{bmatrix} = \left(\mathbf{U}^T\mathbf{U}\right)^{-1}\mathbf{V}, \tag{50}$$

where $\mathbf{U} = [U_1, U_2, \ldots, U_M]^T$ and $\mathbf{V} = [V_1, V_2, \ldots, V_M]^T$. By omitting the sensor index for simplicity, the vector elements in $\mathbf{U}$ and $\mathbf{V}$ are given by

$$U = \begin{bmatrix} -\tan(m_\varphi) & 1 & 0 \\ 1 & 0 & -\sin(m_\varphi)\tan(m_\theta) \\ 0 & 1 & -\cos(m_\varphi)\tan(m_\theta) \end{bmatrix}, \tag{51}$$

$$V = \begin{bmatrix} Y - X\tan(m_\varphi) \\ X - Z\sin(m_\varphi)\tan(m_\theta) \\ Y - Z\cos(m_\varphi)\tan(m_\theta) \end{bmatrix}. \tag{52}$$

B. SIMULATION RESULTS

In this subsection, the simulation results based on the proposed technique are provided for detecting the single-target position. Note that the coordinate unit in this paper is always in meter. First of all, an anonymous target is assumed to be located at $g = [x, y, z]^T$, with each of the coordinate dimensions x, y and $z \in (0, 100)$. There are 4 distributed sensors at the border of the sensing area, and their positions are shown in Table 2.

TABLE 2. Sensor positions (meter) for single-target.

Index \ Coordinate	x	y	z
Sensor 1	50	0	0
Sensor 2	50	100	50
Sensor 3	100	50	100
Sensor 4	0	50	100

According the assumptions described above, the obtained DOAs at each sensor suffer from Gaussian measurement errors. In this simulation, the standard deviations σ_φ and σ_θ are set at 5°, 10°, 15° and 20°, with the snapshot number $L = 500$. Note that in practice, σ_φ and σ_θ may differ, not only at the same sensor, but also among different sensors. However, in order to capture the performance tendency of their effects, the DOA measurements at all sensors are assumed to have the same standard deviation in the simulations.

A detection trajectory using the proposed technique is shown in Fig. 3, with $\sigma_\varphi/\sigma_\theta = 5°$, and the initial guess is set at (0, 0, 0). It is found that within around 5 iterations, the trajectory converges into a point which is very close to the true target position at (76, 62, 81). Since the RMSE result depends on the target position, 1000 targets are randomly generated within the sensing area to calculate the average RMSE performances. Fig. 4 shows the average RMSEs versus iteration times, where the standard deviation of the measurement error is set as the parameter, and the

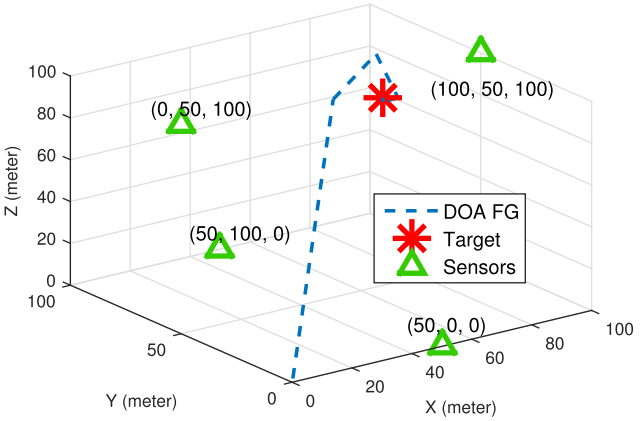

FIGURE 3. Trajectory in 3D for the single-target detection.

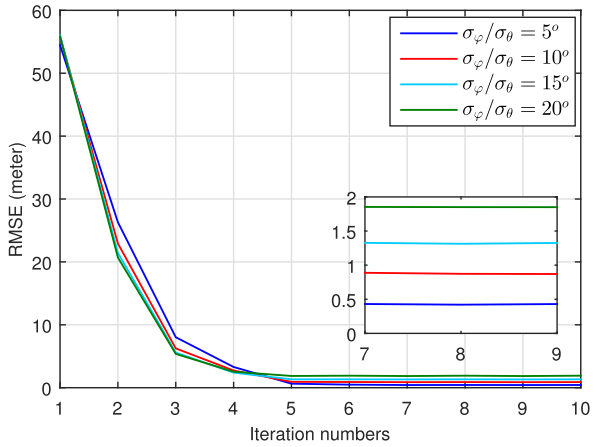

FIGURE 4. Average RMSE versus iterations for 3D single-target detection with different $\sigma_\varphi/\sigma_\theta$.

snapshot number L is fixed at 500. It has been shown that the average RMSE curves converge after around 5-6 iterations. Obviously, the smaller the standard deviation, the lower the average RMSEs. However, even in the case $\sigma_\varphi/\sigma_\theta = 20°$, the proposed technique can achieve an average RMSE less than 2 meter.

Besides the iteration time, the system performance is also affected by the snapshot number L, since it determines the mean and the variance of the measurement error. The value of L maybe limited in practice, and hence it is meaningful to evaluate its impact on the average RMSE. Fig. 5 shows the average RMSE versus $\sigma_\varphi/\sigma_\theta$, where the iteration time is fixed at 10, and the snapshot number L is set as a parameter. Obviously, the larger the L value, the better the performance, in terms of both the simulated average RMSEs and the CRLBs. The effect of L is also found less significant when the standard deviation of the error is small. Moreover, it can be seen that the average RMSEs obtained by simulations are very close to the corresponding CRLBs derived in (48), especially when L is large. With $L = 1000$, the gap is only around

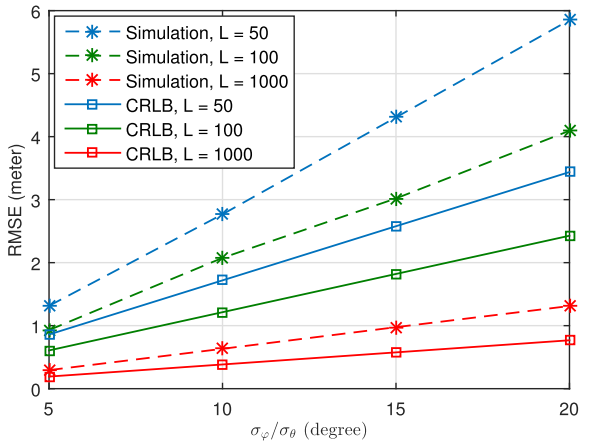

FIGURE 5. Average RMSE versus standard deviation for 3D single-target detection, with L being the parameter.

0.5 meter even when $\sigma_\varphi/\sigma_\theta = 20°$, which demonstrates the high accuracy of our proposed algorithm.

Finally, the proposed FG algorithm is compared to the conventional linear LS approach in terms of the average RMSEs, and the results are shown in Fig. 6. Clearly, the proposed FG algorithm outperforms the conventional LS approach. With $L = 500$, roughly 1 meter improvement of the detection accuracy can be observed with the proposed FG algorithm. In this case, the gaps between the average RMSEs obtained by simulations and the CRLBs are found to be very small, i.e., between 0.15 meter with $\sigma_\varphi/\sigma_\theta = 5°$, and 0.8 meter with $\sigma_\varphi/\sigma_\theta = 20°$.

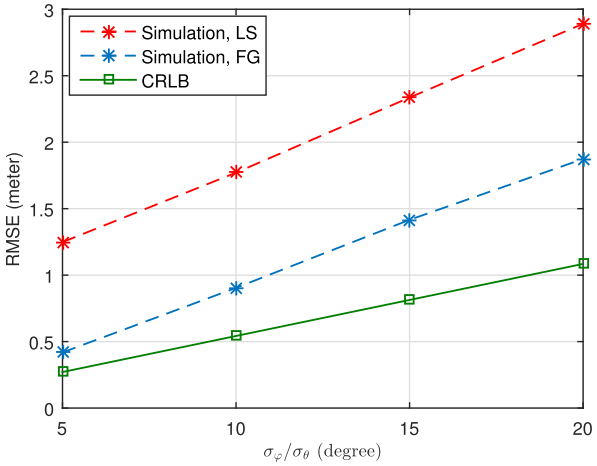

FIGURE 6. Average RMSE comparison between FG and LS for 3D the single-target detection.

VI. GEOLOCATION FOR MULTIPLE TARGETS

A. SENSOR SEPARATION ALGORITHM

In this section, a DOA-based multi-target geolocation is investigated. Even though each sensor is assumed to be capable of measuring the DOAs of different targets, the difficulty lies in the target-DOA matching among distributed sensors. Since the matching between the anonymous targets and their DOAs is a highly combinatory problem, the brute force approach may be intuitively applicable, but it requires heavy computational complexity. Instead, a very simple but yet useful sensor separation algorithm is proposed, which is detailed below. Note that the proposed algorithm is only empirical, which does not aim to provide the optimal estimating results [30].

Let's start with a basic 2D two-target scenario, where the sensors are located on the circle surrounding the two targets, as shown in Fig. 7. $\bar{\varphi}_i^1$ and $\bar{\varphi}_i^2$ are the mean values derived from the two measured DOAs at the *i-th* sensor from the two targets, with the decreasing order $\bar{\varphi}_i^1 > \bar{\varphi}_i^2$. Note that $\bar{\varphi}_i^1$ and $\bar{\varphi}_j^1$ from the i-th and the j-th sensor may not correspond to the same target, because the superscript denotes only the value-ordering of the observed mean DOAs. A sensor separation algorithm is proposed in this paper to distinguish the two DOAs from the two targets. Specifically, this algorithm aims

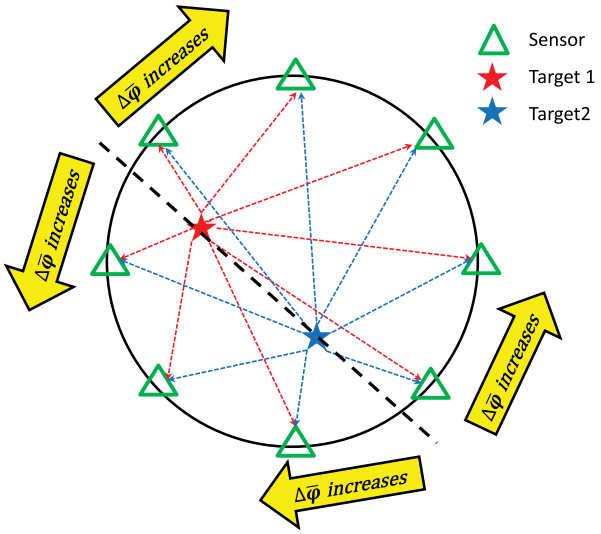

FIGURE 7. Sensor separation for 2D two-target detection.

Algorithm 1 Pseudocode of the Sensor Separation Algorithm for Two-Target

Initialization: $S = \{1, 2, \ldots, M\}$, $S_1 = S_2 = R = \varnothing$;
for i = *1:M* **do**
  $[\bar{\varphi}_i^1, \bar{\varphi}_i^2]$ = sort(two DOAs measured at sensor i) in decreasing order;
  $\Delta\bar{\varphi}_i = \bar{\varphi}_i^1 - \bar{\varphi}_i^2$;
end
$\Delta\bar{\varphi}_0 = \bar{\varphi}_M$;
$\Delta\bar{\varphi}_{M+1} = \bar{\varphi}_1$;
for i = *1:M* **do**
  if $\Delta\bar{\varphi}_i < \Delta\bar{\varphi}_{i-1}$ and $\Delta\bar{\varphi}_i < \Delta\bar{\varphi}_{i+1}$ **then**
    Put i into set R;
  end
end
$S_1 = \{R(1) : 1 : R(\text{end})\}$;
$S_2 = S - S_1$;
$S_1 = S_1 - R$;

to separate the total sensors into two sub-sets, i.e., S_1 and S_2, such that $\bar{\varphi}_{S_1}^1$ and $\bar{\varphi}_{S_2}^2$ are supposed to be from one target, while $\bar{\varphi}_{S_1}^2$ and $\bar{\varphi}_{S_2}^1$ are from the other. To realize such separation, the fusion center compares mean values of the differential DOAs between the neighboring sensors, and finds those which are smaller than their neighbors in both clockwise and counter-clockwise directions. By doing that, if the sensor density is large enough, two sensors can be always found satisfying the condition stated above and therefore dividing the total sensors. However, in practice, there could be only one sensor being found satisfying such condition due to the low density of sensor distribution. In this case, all sensors belong to the same sub-set, i.e., $\bar{\varphi}_S^1$ and $\bar{\varphi}_S^2$ are associated with the DOAs from one and the other targets, receptively. Noted that the sensors used for dividing the sub-sets should be excluded from the following detection due to two reasons: (1) it is difficult to decide which sub-set they are in since their locations are near the border of the sub-sets; (2) the correlation between the two DOAs is supposed to be very large, such that the estimated PDF from the histogram measurement may not be sufficiently accurate. The pseudocode realization of this algorithm is presented in Algorithm 1 as follows.

The extension of the sensor separation algorithm to 2D three-target geolocation is also provided in this section, as illustrated in Fig. 8. Assume that the i-th sensor observes three DOAs with the mean values being $\bar{\varphi}_i^1$, $\bar{\varphi}_i^2$ and $\bar{\varphi}_i^3$ from three targets, where $\bar{\varphi}_i^1 > \bar{\varphi}_i^2 > \bar{\varphi}_i^3$. Two differential mean DOAs $\Delta\bar{\varphi}_i^1 = \left|\bar{\varphi}_i^1 - \bar{\varphi}_i^2\right|$ and $\Delta\bar{\varphi}_i^2 = \left|\bar{\varphi}_i^2 - \bar{\varphi}_i^3\right|$ are calculated for each sensor, based on which the total sensors can be theoretically divided into 6 sub-sets, if the targets are not in a line and the sensor density is sufficiently large. The same as in the two-target case, sensors belonging to the same sub-set can be used for three-target detection with the same target-DOAs matching, i.e., the same target corresponds to the same DOA increasing/decreasing ordering. The proposed sensor separation algorithm for 2D three-target is detailed

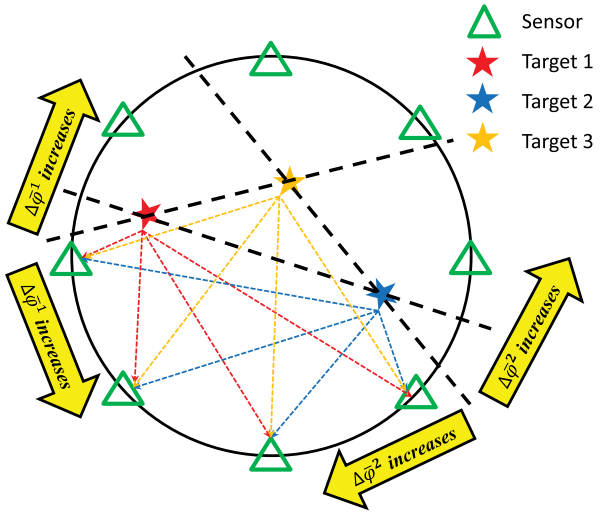

FIGURE 8. Sensor separation for 2D three-target detection.

in Algorithm 2. Similarly, this idea can be extended to the cases with more than three targets, which will not be detailed in this paper. It can be clearly understood that more densely distributed sensors yield higher estimation accuracy with the proposed sensor separation algorithm, especially when the number of targets is large.

According to the assumptions described above, at each sensor, the azimuth is always paired with its corresponding elevation measured from the same target in 3D. Theoretically, given multiple distributed sensors, the target-DOAs matching can be conducted by either the azimuth or the elevation domains. However, it is impossible to use elevation alone to sort the DOAs, since in general the elevation does not separate the targets in height. Instead, the target-DOAs matching should first rely on the azimuth. Specifically, the proposed sensor separation algorithm described above can still be

Algorithm 2 Pseudocode of Sensor Separation Algorithm for Three-Target

Initialization: $S = \{1, 2, \ldots, M\}$, $T = \varnothing$;
for $i = 1 : M$ **do**
  $[\bar{\varphi}_i^1, \bar{\varphi}_i^2, \bar{\varphi}_i^3]$ = sort(three DOAs measured at sensor i) in decreasing order;
  $\Delta\bar{\varphi}_i^1 = \bar{\varphi}_i^1 - \bar{\varphi}_i^2$;
  $\Delta\bar{\varphi}_i^2 = \bar{\varphi}_i^2 - \bar{\varphi}_i^3$;
  $\bar{\Delta}_i = |\Delta\bar{\varphi}_i^1 - \bar{\varphi}_i^2|$;
end
$\bar{\Delta}_0 = \bar{\Delta}_M$;
$\bar{\Delta}_{M+1} = \bar{\Delta}_1$;
for $i = 1 : M$ **do**
  if $\bar{\Delta}_i < \bar{\Delta}_{i-1}$ and $\bar{\Delta}_i < \bar{\Delta}_{i+1}$ **then**
    Put i into set T;
  end
end
t = length(T);
$S_1 = S_2 = \ldots = S_t = \varnothing$;
for $i = 1 : t$ **do**
  put i into S_i;
  $j_1 = T(i) - 1$;
  $j_2 = T(i) + 1$;
  while $\left\{\Delta\bar{\varphi}_{j_1}^1 > \Delta\bar{\varphi}_{j_1-1}^1 \text{ or } \Delta\bar{\varphi}_{j_1}^1 > \Delta\bar{\varphi}_{j_1+1}^1\right\}$ and $\left\{\Delta\bar{\varphi}_{j_1}^2 > \Delta\bar{\varphi}_{j_1-1}^2 \text{ or } \Delta\bar{\varphi}_{j_1}^2 > \Delta\bar{\varphi}_{j_1+1}^2\right\}$ **do**
    Put j_1 into set S_i;
    $j_1 = j_1 - 1$;
    if $j_1 == 0$ **then**
      $j_1 = M$;
    end
  end
  while $\left\{\Delta\bar{\varphi}_{j_2}^1 > \Delta\bar{\varphi}_{j_2-1}^1 \text{ or } \Delta\bar{\varphi}_{j_2}^1 > \Delta\bar{\varphi}_{j_2+1}^1\right\}$ and $\left\{\Delta\bar{\varphi}_{j_2}^2 > \Delta\bar{\varphi}_{j_2-1}^2 \text{ or } \Delta\bar{\varphi}_{j_2}^2 > \Delta\bar{\varphi}_{j_2+1}^2\right\}$ **do**
    Put j_2 into set S_i;
    $j_2 = j_2 + 1$;
    if $j_2 == M + 1$ **then**
      $j_2 = 1$;
    end
  end
end

utilized, by simply projecting the sensors and the targets onto the 2D X-Y plane. However, in the case that the projected multiple targets have very close positions at the X-Y plane, the measured elevations will directly separate the targets by their heights, and therefore can provide us the target-DOAs matching information. Thereby, the multi-target geolocation in 3D can be similarly decomposed into multiple independent 3D single-target detections.

B. MULTI-TARGET SIMULATIONS

In this section, the multi-target geolocation is simulated based on the proposed technique. For the initialization, 8 sensors are assumed to be allocated on the edge of the 3D sensing area, with their locations given in Table 3. Multi-target detection is simulated in both 2D and 3D. In the case of 2D, only x and y columns from Table 3 are used for the sensor positions.

TABLE 3. Sensor position (meter) setup in 3D.

Index \ Coordinate	x	y	z
Sensor 1	100	200	10
Sensor 2	170.7	170.7	140
Sensor 3	200	100	20
Sensor 4	170.7	29.3	160
Sensor 5	100	0	80
Sensor 6	29.3	29.3	170
Sensor 7	0	100	30
Sensor 8	29.3	170.7	150

First of all, a trajectory of 2D detection is shown in Fig. 9, with $L = 500, \sigma_\varphi = 5°$ and the two target positions being (150, 140) and (130, 40). By utilizing the proposed Algorithm 1, sensor 2 and sensor 5 are selected to separate the total sensors, i.e., $R = \{2, 5\}$. The two sub-sets of sensors can then be obtained by $S_1 = \{3, 4\}$ and $S_2 = \{1, 6, 7, 8\}$, where the sensors in R are excluded. The proposed algorithm concludes that the mean DOAs from S_1 and S_2 having different increasing/decreasing orders can be used to detect the same target. Hence, after separating the sensors, the detection of two targets can be independently conducted, with their corresponding DOAs only. It can be clearly seen in Fig. 9 that with around 3 or 4 iterations for each target, the estimations converge into the points very close to the true target positions.

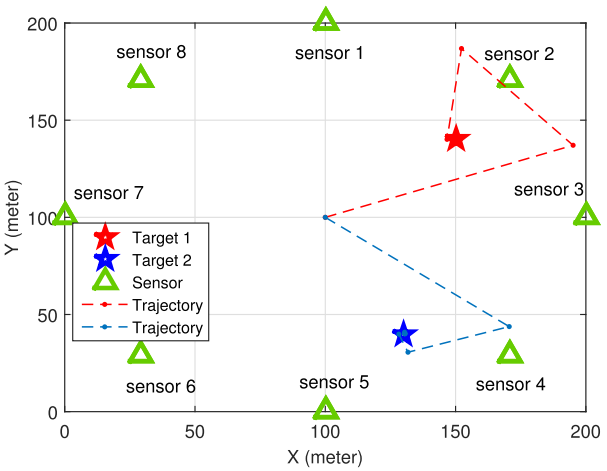

FIGURE 9. Trajectories in 2D for two-target detection.

Fig. 10 shows the case of 3D geolocation with two targets locating at (75, 142, 115) and (150, 50, 108). First of all, the sensor separation algorithm is performed over the azimuth dimension, which projects the positions of all objects onto the 2D X-Y plane. According to our simulation results,

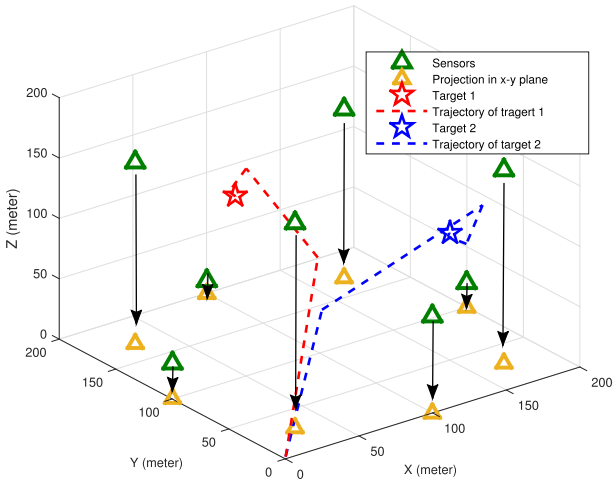

FIGURE 10. Trajectories in 3D for two-target detection, with the sensor separation performed in 2D X-Y plane.

$R = \{4, 8\}$ is obtained, with $S_1 = \{5, 6, 7\}$ and $S_2 = \{1, 2, 3\}$. Consequently, the convergence behavior of the 3D trajectories can be well observed. Due to the similarity between Algorithm 1 and 2, the trajectory for three-target geolocation is not shown in this paper.

Moreover, the average RMSEs are verified through simulations and compared to the CRLBs, as shown in Fig. 11. 1000 targets are randomly generated with the x, y and z-coordinate in (30, 170). It is found from Fig. 11 that the CRLB of the two-target case increases by roughly 0.25 meter compared to that of the single-target case, if $\sigma_\varphi/\sigma_\theta = 20°$. When the target number increases to three, a larger CRLB gap can be observed compared to that of the two-target case. Furthermore, the average RMSEs obtained through simulations in the three cases exhibit almost the same tendencies of their CRLBs. It should be noted that the performance loss in our proposed multi-target geolocation is due to the exclusion of sensors from the sensor sub-sets, which are not

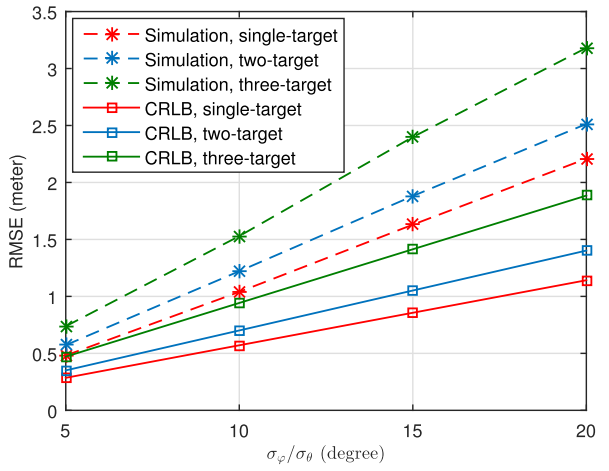

FIGURE 11. Average RMSE versus standard deviation for 3D multi-target detection.

used in the detection. Therefore, the larger the target number, the more sensors need to be excluded. That is the reason for the loss found in the three-target case being more severe than that of the two-target, with the same sensor setup in this simulation. This observation invokes a reasonable conclusion that, the multi-target geolocation performance may further be improved with more densely distributed sensors, if a larger number of target is aimed at.

VII. CONCLUSION

This paper has proposed a DOA-based 3D geolocation technique for anonymous multiple targets using a FG algorithm. It has been shown that the proposed technique outperforms the conventional LS approach in terms of the average RMSE. Due to the assumption of multiple distributed sensors, the matching between DOAs, measured at different sensors, and their originating target is unknown, which is referred to as the target-DOAs matching problem. This problem has been solved by the proposed sensor separation algorithm, such that the conventional target-specific identification techniques, e.g., reference signal, are avoided. Moreover, the CRLB of the proposed system has been mathematically derived. The performances of the our technique have been evaluated by simulations, which are shown very close to the CRLB. Up to our best knowledge, this paper for the first time addressed a target-DOAs matching problem, for solving the DOA-based 3D multi-target geolocation using FG algorithm. Our next research target includes developing tracking capability based on the proposed technique.

APPENDIX
CRLB DERIVATION

The CRLB derivation of the proposed DOA-based 3D geolocation system is presented in this appendix. According to the Gaussian assumptions shown in (8) and (9), the PDFs of the measured DOA samples can be given by

$$p(\hat{\varphi}) = \prod_{l=1}^{L} \frac{1}{\sqrt{2\pi\sigma_\varphi^2}} \exp\left[-\frac{1}{2\sigma_\varphi^2}\left(\hat{\varphi}_l - \varphi\right)^2\right], \quad (53)$$

$$p(\hat{\theta}) = \prod_{l=1}^{L} \frac{1}{\sqrt{2\pi\sigma_\theta^2}} \exp\left[-\frac{1}{2\sigma_\theta^2}\left(\hat{\theta}_l - \theta\right)^2\right], \quad (54)$$

where the true DOAs can be written by

$$\varphi = \arctan\left(\frac{Y-y}{X-x}\right), \quad (55)$$

$$\theta = \arctan\left(\frac{Z-z}{\sqrt{(X-x)^2+(Y-y)^2}}\right). \quad (56)$$

Let $\hat{A}$ represent the measured DOA variable including both $\hat{\varphi}$ and $\hat{\theta}$, the fisher information function can be expressed by

$$E\left[\left(\frac{\partial}{\partial A}\ln p(\hat{A})\right)^2\right] = -E\left[\frac{\partial^2}{\partial A^2}\ln p(\hat{A})\right]. \quad (57)$$

According to (53) and (54),

$$\frac{\partial^2}{\partial A^2}\ln p(\hat{A}) = -\frac{L}{\sigma_A^2}. \tag{58}$$

Therefore, the FIM can be further derived by

$$\begin{aligned} F(g) &= \frac{\partial A}{\partial g}^T E\left[\left(\frac{\partial}{\partial A}\ln p(\hat{A})\right)^T\left(\frac{\partial}{\partial A}\ln p(\hat{A})\right)\right]\frac{\partial A}{\partial g} \\ &= \frac{\partial A}{\partial g}^T E\left[\left(\frac{\partial}{\partial A}\ln p(\hat{A})\right)^2\right]\frac{\partial A}{\partial g} \\ &= \frac{\partial A}{\partial g}^T\left[\frac{L}{\sigma_A^2}\right]\frac{\partial A}{\partial g}. \end{aligned} \tag{59}$$

The Jacobian matrix in (59) is given by

$$\mathbf{J} = \frac{\partial A}{\partial g} = \begin{bmatrix} \frac{\partial \varphi_1}{\partial x} & \frac{\partial \varphi_1}{\partial y} & \frac{\partial \varphi_1}{\partial z} \\ \frac{\partial \varphi_2}{\partial x} & \frac{\partial \varphi_2}{\partial y} & \frac{\partial \varphi_2}{\partial z} \\ \vdots & \vdots & \vdots \\ \frac{\partial \theta_1}{\partial x} & \frac{\partial \theta_1}{\partial y} & \frac{\partial \theta_1}{\partial z} \\ \frac{\partial \theta_2}{\partial x} & \frac{\partial \theta_2}{\partial y} & \frac{\partial \theta_2}{\partial z} \\ \vdots & \vdots & \vdots \end{bmatrix}, \tag{60}$$

where

$$\frac{\partial \varphi}{\partial x} = \frac{\Delta y}{\Delta xy}, \tag{61}$$

$$\frac{\partial \varphi}{\partial y} = -\frac{\Delta x}{\Delta xy}, \tag{62}$$

$$\frac{\partial \varphi}{\partial z} = 0, \tag{63}$$

$$\frac{\partial \theta}{\partial x} = \frac{\Delta x \Delta z}{\Delta xy \Delta xyz^2}, \tag{64}$$

$$\frac{\partial \theta}{\partial y} = \frac{\Delta y \Delta z}{\Delta xy \Delta xyz^2}, \tag{65}$$

$$\frac{\partial \theta}{\partial z} = \frac{-\Delta xy}{\Delta xyz^2}. \tag{66}$$

The Euclidean distance between the sensor and the target in 3D space is denoted by Δxyz, and Δxy represents the projected distance of Δxyz on the X-Y plane.

REFERENCES

[1] W. Yahui and G. Xiaoran, "The study of location technology based on wireless sensor networks in smart city," in *Proc. 12th IEEE Int. Conf. Control Automat. (ICCA)*, Jun. 2016, pp. 848–853.
[2] Y. Li, L. Yang, S. Han, X. Wang, and F.-Y. Wang, "When LPWAN meets ITS: Evaluation of low power wide area networks for V2X communications," in *Proc. 21st Int. Conf. Intell. Transp. Syst. (ITSC)*, Nov. 2018, pp. 473–478.
[3] Y. Mao, C. You, J. Zhang, K. Huang, and K. B. Letaief, "A survey on mobile edge computing: The communication perspective," *IEEE Commun. Surveys Tuts.*, vol. 19, no. 4, pp. 2322–2358, 4th Quart., 2017.
[4] W. Shi, J. Cao, Q. Zhang, Y. Li, and L. Xu, "Edge computing: Vision and challenges," *IEEE Internet Things J.*, vol. 3, no. 5, pp. 637–646, Oct. 2016.
[5] J.-C. Chen, C.-S. Maa, and J.-T. Chen, "Factor graphs for mobile position location," in *Proc. IEEE Int. Conf. Acoust., Speech, Signal Process.*, vol. 2, Apr. 2003, pp. 393–396.
[6] A. P. Worthen and W. E. Stark, "Unified design of iterative receivers using factor graphs," *IEEE Trans. Inf. Theory*, vol. 47, no. 2, pp. 843–849, Feb. 2001.
[7] M. R. K. Aziz, K. Anwar, and T. Matsumoto, "A new DOA-based factor graph geolocation technique for detection of unknown radio wave emitter position using the first-order Taylor series approximation," *EURASIP J. Wireless Commun. Netw.*, vol. 2016, no. 1, p. 189, Dec. 2016.
[8] F. Mekelleche and H. Haffaf, "Classification and comparison of range-based localization techniques in wireless sensor networks," *J. Commun.*, vol. 12, pp. 221–227, Apr. 2017.
[9] H.-L. Jhi, J.-C. Chen, C.-H. Lin, and C.-T. Huang, "A factor-graph-based TOA location estimator," *IEEE Trans. Wireless Commun.*, vol. 11, no. 5, pp. 1764–1773, May 2012.
[10] C. T. Huang, C. H. Wu, Y. N. Lee, and J. T. Chen, "A novel indoor RSS-based position location algorithm using factor graphs," *IEEE Trans. Wireless Commun.*, vol. 8, no. 6, pp. 3050–3058, Jun. 2009.
[11] S. N. Karimah, M. R. K. Aziz, and T. Matsumoto, "A hybrid TOA and RSS-based factor graph for wireless geolocation technique," in *Proc. IEEE 12th Int. Colloq. Signal Process., Appl. (CSPA)*, Mar. 2016, pp. 140–145.
[12] C. Mensing and S. Plass, "TDOA positioning based on factor graphs," in *Proc. IEEE 17th Int. Symp. Pers., Indoor, Mobile Radio Commun. (PIMRC)*, Sep. 2006, pp. 1–5.
[13] J.-C. Chen, P. Ting, C.-S. Maa, and J.-T. Chen, "Wireless geolocation with TOA/AOA measurements using factor graph and sum-product algorithm," in *Proc. IEEE VTC-Fall*, vol. 5, Sep. 2004, pp. 3526–3529.
[14] R. Levorato and E. Pagello, "DOA acoustic source localization in mobile robot sensor networks," in *Proc. IEEE Int. Conf. Auton. Robot Syst., Competitions*, Apr. 2015, pp. 71–76.
[15] H. Wymeersch, G. Seco-Granados, G. Destino, D. Dardari, and F. Tufvesson, "5G mmWave positioning for vehicular networks," *IEEE Wireless Commun.*, vol. 24, no. 6, pp. 80–86, Dec. 2017.
[16] J. Chen, S. Guan, Y. Tong, and L. Yan, "Two-dimensional direction of arrival estimation for improved archimedean spiral array with MUSIC algorithm," *IEEE Access*, vol. 6, pp. 49740–49745, Aug. 2018.
[17] M. L. Bencheikh and Y. Wang, "Joint DOD-DOA estimation using combined ESPRIT-MUSIC approach in MIMO radar," *Electron. Lett.*, vol. 46, no. 15, pp. 1081–1083, Jul. 2010.
[18] B. R. Karthikeyan, G. R. Kadambi, and Y. A. Vershinin, "A formulation of 1-D search technique for 2-D DOA estimation using orthogonally polarized components of linear array," *IEEE Antennas Wireless Propag. Lett.*, vol. 14, pp. 1117–1120, 2015.
[19] G. Zhao, G. Shi, F. Shen, X. Luo, and Y. Niu, "A sparse representation-based DOA estimation algorithm with separable observation model," *IEEE Antennas Wireless Propag. Lett.*, vol. 14, pp. 1586–1589, 2015.
[20] S. Gong, H. Xiong, M. Peng, X. Ding, and H. Tang, "Joint DOD and DOA estimation for bistatic multiple-input multiple-output radar target discrimination based on improved unitary ESPRIT method," *IET Commun.*, vol. 12, no. 12, pp. 1397–1405, Jul. 2018.
[21] Y. Wei and X. Guo, "Pair-matching method by signal covariance matrices for 2D-DOA estimation," *IEEE Antennas Wireless Propag. Lett.*, vol. 13, no. 6, pp. 1199–1202, Jun. 2014.
[22] J.-C. Chen, Y.-C. Wang, C.-S. Maa, and J.-T. Chen, "Network-side mobile position location using factor graphs," *IEEE Trans. Wireless Commun.*, vol. 5, no. 10, pp. 2696–2704, Oct. 2006.
[23] U. K. Singh, V. Bhatia, and A. K. Mishra, "Multiple target detection and estimation of range and Doppler for OFDM-RADAR system," in *Proc. 4th Int. Conf. Signal Process., Integr. Netw.*, Feb. 2017, pp. 27–32.
[24] Z. Cao, P. Chen, Z. Chen, and Y. Jin, "DOA estimation for multiple targets in MIMO radar with nonorthogonal signals," *Math. Problems Eng.*, vol. 2018, Jul. 2018, Art. no. 6465856.
[25] R. Zhang, J. Liu, X. Du, B. Li, and M. Guizani, "AOA-based three-dimensional multi-target localization in industrial WSNs for LOS conditions," *Sensors*, vol. 18, no. 8, p. 2727, Aug. 2018.
[26] F. Meyer, P. Braca, P. Willett, and F. Hlawatsch, "A scalable algorithm for tracking an unknown number of targets using multiple sensors," *IEEE Trans. Signal Process.*, vol. 65, no. 13, pp. 3478–3493, Jul. 2017.
[27] M. Frohle, C. Lindberg, and H. Wymeersch, "Cooperative localization of vehicles without inter-vehicle measurements," in *Proc. IEEE Wireless Commun., Netw. Conf. (WCNC)*, Apr. 2018, pp. 1–6.

[28] K. W. Cheung, H. C. So, W.-K. Ma, and Y. T. Chan, "Least squares algorithms for time-of-arrival-based mobile location," *IEEE Trans. Signal Process.*, vol. 52, no. 4, pp. 1121–1130, Apr. 2004.
[29] H.-A. Loeliger, J. Dauwels, J. Hu, S. Korl, L. Ping, and F. R. Kschischang, "The factor graph approach to model-based signal processing," *Proc. IEEE*, vol. 95, no. 6, pp. 1295–1322, Jun. 2007.
[30] D. Moreno-Salinas, A. M. Pascoal, and J. Aranda, "Optimal sensor placement for multiple target positioning with range-only measurements in two-dimensional scenarios," *Sensors*, vol. 13, no. 8, pp. 10674–10710, Aug. 2013.

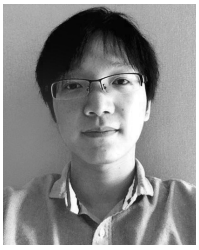

MENG CHENG (S'12–M'16) received the B.Eng. degree in telecommunication engineering from the Anhui University of Technology, Anhui, China, in 2009, the M.Sc. degree (Hons.) in wireless communications from the University of Southampton, Southampton, U.K., in 2010, and the Ph.D. degree in information science from the Japan Advanced Institute of Science and Technology (JAIST), Ishikawa, Japan, in 2014. He has served as a 5G Research Engineer with the Shanghai Research Center, Huawei Technologies Company Ltd., from 2014 to 2017. After that, he returned to JAIST as a Postdoctoral Researcher. His research interests include network information theory, non-orthogonal multiple access (NOMA), iterative coding/decoding, and wireless geolocation techniques.

MUHAMMAD REZA KAHAR AZIZ (S'13–M'17) was born in Bandar Lampung, Indonesia, in 1981. He received the bachelor's and master's degrees *(cum laude)* in electrical engineering (telecommunications) with the Institut Teknologi Bandung (ITB), Bandung, Indonesia, in 2004 and 2012, respectively, and the Ph.D. degree in information science from the Japan Advanced Institute of Science and Technology (JAIST), Ishikawa, Japan, in 2016.

In 2005, he joined the MERCATOR Summer School, University of Duisburg Essen (UDE) at Universitas Indonesia (UI) Campus, Jakarta, Indonesia. From 2004 to 2005, he was a Microwave Radio Service Engineer and a Project Coordinator in Siemens Indonesia. Then, he was with Ericsson Indonesia (EID) as a Broadband Solution Engineer in wireless and optical transport, from 2005 to 2010, where he was also selected as the Ericsson Microwave Radio Champion for Indonesia Region. After that, he served as Teaching Assistant with ITB, in 2011, and an Adjunct Lecturer with Institut Teknologi Telkom (ITT). Since 2012, he has been with the Institut Teknologi Sumatera (ITERA), Lampung, Indonesia, as a Teaching Staff. He also received the Graduate Research Program Scholarship (GRP) and Doctor Research Fellowship (DRF) from JAIST, from 2013 to 2016. His research interests include wireless communication systems, signal processing, information theory, radio geolocation, factor graph, antennas, and electromagnetics.

Dr. Aziz has received the award of 10% top performer Ericsson Indonesia employee, in 2009, and ITB Voucher Scholarship, in 2011. Furthermore, he has received the Best Paper Award from the Nineth Asia Modeling Symposium (AMS), in 2015, Kuala Lumpur, Malaysia, and the Second Symposium of Future Telecommunication and Technologies (SOFTT), in 2018, Bandung, Indonesia. He also received the JAIST Foundation Research Grant for Students to attend the European Wireless Conference 2016, Oulu, Finland. He also received research grant of Hibah Mandiri from ITERA, in 2017. He is serving as a Reviewer and a TPC member of IEEE conferences, including, ICC, Globecom, VTC, and others, and several journals including the IEEE TVT.

TAD MATSUMOTO (S'84–M'98–F'10) received the B.S. and M.S. degrees in electrical engineering under the mentorship of Prof. S.-I. Takahashi, and the Ph.D. degree in electrical engineering under the supervision of Prof. M. Nakagawa from Keio University, Yokohama, Japan, in 1978, 1980, and 1991, respectively.

He joined Nippon Telegraph and Telephone Corporation (NTT), in 1980, where he was involved in a lot of research and development projects mobile wireless communications systems. In 1992, he transferred to NTT DoCoMo, where he researched on code-division multiple-access techniques for mobile communication systems. In 1994, he transferred to NTT America, where he served as a Senior Technical Advisor of a joint project between NTT and NEXTEL Communications. In 1996, he returned to NTT DoCoMo, where he served as the Head of the Radio Signal Processing Laboratory, until 2001. He researched on adaptive signal processing, multiple-input–multiple-output turbo signal detection, interference cancellation, and space-time coding techniques for broadband mobile communications. In 2002, he moved to the University of Oulu, Finland, where he served as a Professor with the Centre for Wireless Communications. In 2006, he has served as a Visiting Professor with the Ilmenau University of Technology, Ilmenau, Germany, supported by the German MERCATOR Visiting Professorship Program. Since 2007, he has been serving as a Professor with the Japan Advanced Institute of Science and Technology, Japan, while also keeping a cross-appointment position with the University of Oulu.

Dr. Matsumoto is a member of the IEICE. He has led a lot of projects supported by the Academy of Finland, European FP7, and the Japan Society for the Promotion of Science and Japanese private companies. He has been appointed as a Finland Distinguished Professor, from 2008 to 2012, supported by the Finnish National Technology Agency (Tekes) and Finnish Academy, under which he preserves the rights to participate in and apply for European and Finnish National Projects. He was a recipient of the IEEE VTS Outstanding Service Award, in 2001, the Nokia Foundation Visiting Fellow Scholarship Award, in 2002, the IEEE Japan Council Award for Distinguished Service to the Society, in 2006, the IEEE Vehicular Technology Society James R. Evans Avant Garde Award, in 2006, the Thuringen State Research Award for Advanced Applied Science, in 2006, the 2007 Best Paper Award of the Institute of Electrical, Communication, and Information Engineers of Japan, in 2008, the Telecom System Technology Award from the Telecommunications Advancement Foundation, in 2009, the IEEE Communication Letters Exemplary Reviewer, in 2011, the Nikkei Wireless Japan Award, in 2013, the IEEE VTS Recognition for Outstanding Distinguished Lecturer, in 2016, and the IEEE TRANSACTIONS ON COMMUNICATIONS Exemplary Reviewer, in 2018. He has been serving as an IEEE Vehicular Technology Distinguished Speaker, since 2016.